Bull. Mater. Sci., Vol. 25, No. 7, December 2002, pp. 635–639. © Indian Academy of Sciences.

Fine structures in Fe_3Al alloy layer of a new hot dip aluminized steel

LI YAJIANG*†, WANG JUAN†, ZHANG YONGLAN† and X HOLLY‡

*National Key Laboratory of Advanced Welding Production Technology, Harbin Institute of Technology, Harbin 150001, PR China

†Key Lab of Liquid Structure and Heredity of Materials, Ministry of Education, Shandong University, Jinan 250061, PR China

‡Computer Engineering Department, University of Northern Virginia, VA 20147, USA

MS received 30 August 2002

Abstract. The fine structure in the Fe–Al alloy layer of a new hot dip aluminized steel (HDA) was examined by means of X-ray diffractometry (XRD), electron diffraction technique, etc. The test results indicated that the Fe–Al alloy layer of the new aluminized steel mainly composed of Fe_3Al, FeAl and *a*-Fe (Al) solid solution. There was no brittle phase containing higher aluminum content, such as $FeAl_3$ (59·18% Al) and Fe_2Al_7 (62·93% Al). The tiny cracks and embrittlement, formerly caused by these brittle phases in the conventional aluminum-coated steel, were effectively eliminated. There was no microscopic defect (such as tiny cracks, pores or loose layer) in the coating. This is favourable to resist high temperature oxidation and corrosion of the aluminized steel.

Keywords. Surface alloying; iron aluminides; electron diffraction; X-ray diffraction (XRD).

1. Introduction

The present aluminizing technologies include solid powder method, paste calorized method and hot dip aluminizing (HDA), etc of which HDA technique is one of the most economical techniques for the aluminizing of steel surface in large quantities (Bahadur and Mohanty 1991). The aluminized steel exhibits excellent resistance to oxidation and corrosion, and can substitute for stainless steel or heat-resisting steel in some situations. The aluminized steel has wide applications, owing to its low cost and excellent performance, in the petrochemical industry, electric power and other energy conversion system, etc and has attracted the attention of many investigators (Tjong 1986; Bahadur and Mohanty 1990, 1991; Li *et al* 1995). In different aluminizing technologies, the phase constitution and performance of the Fe–Al alloy layer exhibit large differences.

Some investigators carried out investigation on the aluminizing technology, mechanical properties and corrosion resistance of the aluminized steel (Bahadur and Mohanty 1991; Li and Wang 1992). However, the study of the phase structure in the Fe–Al alloy layer is still scarce, particularly the combination between the phase structure and the base metal at the interface of the coating (Li *et al* 2001). In the engineering application, the damage of the aluminized steel is mostly at the position of the interface joint. Through the analysis, these damages originate mostly from the Fe–Al alloy layer of the aluminized steel. Therefore, this study on the phase structure of the Fe–Al alloy layer has an important application value. By controlling technology parameters, the phase structure and performance in the coating can be improved and service life of the aluminized steel can significantly be enhanced.

2. Experimental

The base metal of the aluminized steel used in this investigation was mild steel (0·18%C), which was aluminized by the hot dip aluminizing technology (HDA). In order to improve the adhesion of the liquid aluminum to the base metal, the surface of the workpiece was treated by 0·5 ~ 1·5% HCl water solution, and then treated by $ZnCl_2$ plus NH_4Cl solution ($ZnCl_2 : NH_4Cl = 3 : 2$) before aluminizing. The crucible electric resistance furnace was heated to 780°C and after all aluminum was melted, the samples of the surface-cleaned low-carbon steel was immersed into the molten aluminum alloy and kept for 10 min, and then the aluminized sample was diffusion annealed (640°C × 30 min). In this process, Al and Fe atoms diffuse into each other and Fe–Al intermetallic compound layer was formed on the surface of the sample. The composition of the aluminum liquid was: 90% Al, 6% Fe, 3% Si and others 1%. Silicon was added into the aluminum liquid in order to make the surface of the Fe–Al alloy layer smooth.

A number of specimens were cut out from the workpiece of the aluminized steel using the line cut machine, and were prepared for metallographic examination. The Al content and the microhardness in the Fe–Al alloy layer were measured in discreet layers by means of

*Author for correspondence

Table 1. Microhardness, aluminum and iron content and main phases in the Fe–Al alloy layer.

Measuring point	Distance from surface (μm)	Region	Al (wt%)	Fe (wt%)	Microhardness	Possible phases
1	0	Surface	36·6	64·0	160	Al_2O_3
2	12	Coating, outer edge	32·7	68·1	240	Fe_3Al + FeAl
3	18	Coating, outer edge	–	–	490	
4	24	Coating, outer edge	–	–	630	
5	32	Coating, middle part	29·2	70·4	820	Fe_2Al_5 + FeAl + Fe_3Al
6	55	Coating, middle part	26·5	73·2	740	
7	68	Coating, middle part	–	–	690	
8	80	Coating	–	–	614	FeAl + Fe_3Al
9	95	Coating	18·8	80·5	588	
10	110	Coating	8·1	91·0	392	
11	130	Coating, boundary with base	1·4	97·8	290	Fe_3Al + *a*-Fe(Al) solid solution
12	140	Base metal	0·3	99·2	260	Ferrite

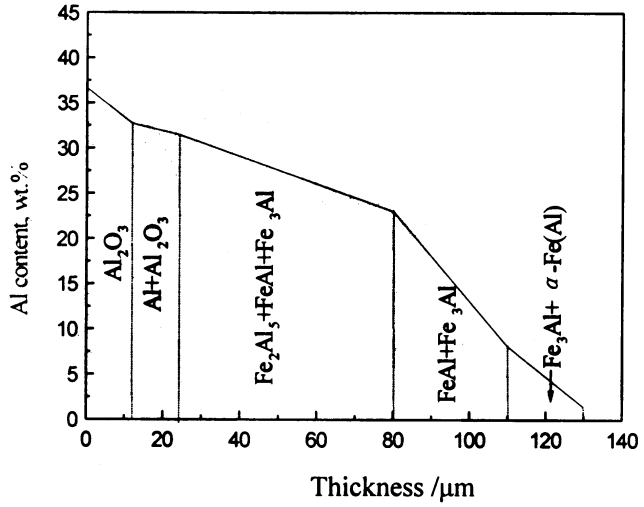

Figure 1. The structural variation in the Fe–Al alloy layer.

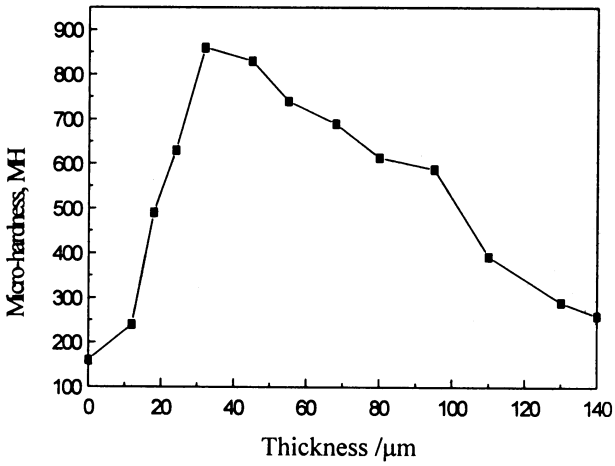

Figure 2. The variation of microhardness with depth in the Fe–Al alloy layer.

electron probe microanalysis (EPMA) and microsclerometer, using a 50 g load and period of 12 s. The phase structure in the Fe–Al alloy layer was analysed by X-ray diffractometer (XRD) using CuK_a radiations. The working voltage was 40 kV and the working current was 150 mA. The Fe–Al alloy layers were cut into 30 μm films and were further etched by the electrolysis spray method. Afterwards, the phase structure of these film samples was analysed by means of transmission electron microscopy (TEM) and electron diffraction technique.

3. Results

3.1 *Thickness and aluminum content in the Fe–Al alloy layer*

After the samples of the aluminized steel were etched by nital, the microstructure of the Fe–Al alloy layer and the base metal were clearly displayed. The metallographic analysis indicated that the thickness of the Fe–Al alloy layer on the surface of the hot dip aluminized steel was about 140 μm.

Microstructure, aluminum content and microhardness in the Fe–Al alloy layer are shown in table 1. The effect of thickness on the phase structure in the Fe–Al alloy layer is shown in figure 1. The change of microhardness with the coating thickness is shown in figure 2. The variation of the microhardness value in the Fe–Al alloy layer was large, indicating that the phase structure and performance in the Fe–Al alloy layer also varied accordingly. The microhardness of the Fe–Al alloy layer was measured from surface to the inside by a microsclerometer. The test results indicated that the microhardness of the surface layer was lower (HV 130 ~ 250), the microhardness of the sub-surface layer was higher (HV 490 ~ 860), and then it reduced gradually.

There was micro roughness phenomenon on the surface of the Fe–Al alloy layer of the aluminized sample. The EPMA analysis indicated that the content of aluminum was 36·6 wt% on the rough surface and 32·7 wt% on the smooth regions.

In order to clarify the phase constitution of the Fe–Al alloy layer and whether or not there is the precipitation of solid aluminum chloride in the coating, the Fe–Al alloy layer was analysed in discreet layers from the surface to the inside by means of EPMA. There was Al concentration gradient along with the thickness direction of the Fe–Al alloy layer after the aluminized sample was treated using diffusion annealing. This made Al atoms diffuse to the base metal through the diffusion layer, and Al content in the Fe–Al alloy layer reduced gradually from the surface layer to inside. According to the microhardness and the EPMA result of the Fe–Al alloy layer and the performance of some Fe–Al intermetallic compounds (see table 2), perhaps phases in the Fe–Al alloy layer were Fe_3Al, FeAl, Fe_2Al_5 and *a*-Fe (Al) solid solution, etc.

The thickness of the Fe–Al alloy layer was determined by the diffusion of Al atom. Al atom continuously diffused in the coating through a series of Fe–Al intermetallic compounds. The growth of the Fe–Al alloy layer was on the interface of the coating and the base metal. With the prolongation of the diffusion time, Al atom diffused continuously to the coating, which made the thickness of the alloy layer grow.

Table 2. Microhardness of intermetallic compounds in the Fe–Al system.

Phase	Al content (wt%) According to phase diagram	Al content (wt%) Chemical analysis	Microhardness
Fe_3Al	13·87	14·04	350
FeAl	32·57	33·64	640
$FeAl_2$	49·13	49·32	1030
Fe_2Al_5	54·71	54·92	820
$FeAl_3$	59·18	59·40	990
Fe_2Al_7	62·93	63·32	1080

3.2 *XRD analysis*

There are a series of intermetallic compounds in the Fe–Al system, such as FeAl, Fe_3Al, $FeAl_2$, $FeAl_3$, Fe_2Al_5, etc. In the range of forming of Fe_3Al, other Fe–Al phase can also be formed. X-ray diffraction diagram in the Fe–Al alloy layer of the new aluminized steel is shown in figure 3. The *d* value corresponding to the diffraction peak in the diffractogram was calculated by means of the computer. The calculated result was compared with the *d* values of FeAl phase, Fe_3Al phase, Fe_2Al_5 phase, *a*-Fe (Al) solid solution and Al_2O_3, published by the Joint Committee on Powder Diffraction Standards (JCPDS) (table 3).

The XRD test result indicated that the Fe–Al alloy layer of the new aluminized steel was composed of *a*-Fe (Al) solid solution, Fe_3Al (13·87% Al), FeAl (32·57% Al), Fe_2Al_5 (54·71% Al) with different proportions and some Al_2O_3 on the surface (table 3). There was no brittle phase containing higher aluminum content, such as $FeAl_3$ (59·18% Al) and Fe_2Al_7 (62·93% Al). With the increase of the depth of Fe–Al alloy layer, the content of Fe_3Al phase and *a*-Fe (Al) solid solution increased. The tiny cracks, embrittlement and deterioration of adhesion, formerly caused by these brittle phases in the conventional aluminum-coated steel, were effectively eliminated. This is favourable for the application of the aluminized steel.

3.3 *TEM analysis*

To clarify the morphology of the phase structure in the Fe–Al alloy layer, the fine structure of the film sample from the Fe–Al alloy layer was analysed by means of TEM and electron diffraction technique. TEM morphology, electron diffraction pattern and schematic diagram in the Fe–Al alloy layer, taken from [211] orientation, are

Table 3. Experimental results of X-ray diffraction for the Fe–Al alloy layer.

Test values	Date from JCPDS											
	Fe_2Al_5			FeAl			Fe_3Al			*a*-Fe(Al)		
d (nm)	*d* (nm)	*hkl*	I/I_0	*d* (nm)	*hkl*	I/I_0	*d* (nm)	*hkl*	I/I_0	*d* (nm)	*hkl*	I/I_0
0·234	–	–	–	–	–	–	–	–	–	–	–	–
0·210	–	–	–	–	–	–	–	–	–	–	–	–
0·203	0·205	130	100	0·204	110	100	0·204	220	100	0·203	110	100
0·192	0·190	400	8	–	–	–	–	–	–	–	–	–
0·188	0·184	202	4	–	–	–	–	–	–	–	–	–
0·170	0·170	–	2	–	–	–	–	–	–	–	–	–
0·164	0·163	330	2	0·167	111	4	0·167	222	10	–	–	–
0·153	0·155	421	2	–	–	–	–	–	–	–	–	–
0·145	–	–	–	–	–	–	–	–	–	–	–	–
0·143	–	–	–	0·145	200	8	0·145	400	80	0·143	200	20
0·131	–	–	–	0·130	210	3	–	–	–	–	–	–
0·117	–	–	–	0·118	211	20	0·118	422	90	0·117	211	30

shown in figure 4 (a, b, c). The electron diffraction pattern of the Fe–Al alloy layer was a series of spots in the regular arrangement.

The black region in the TEM (figure 4a) was Fe_3Al phase and the white region was *a*-Fe (Al) solid solution with body-centred cubic structure (lattice constant is 0·287 nm). Under the TEM, observation and analysis of the phase structure characteristics of the Fe–Al alloy layer indicated that the component phases were composed of inlaid sub-crystal grains. There were some dislocation networks at the boundary of the component phase. No microscopic defects (such as tiny cracks, pores or loose layer) were found in the Fe–Al alloy layer. The test result indicated that the microstructure of the Fe–Al alloy layer with Fe_3Al as main phase structure was compact, which is favourable to resist high temperature oxidation and corrosion of the aluminized steel.

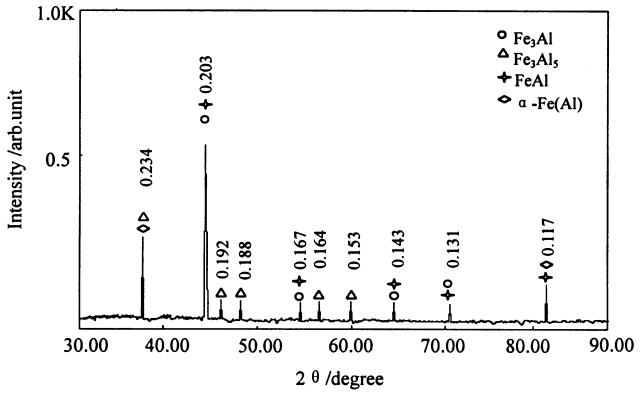

Figure 3. X-ray diffractogram of the Fe–Al alloy layer (diffraction conditions: Cu target, 40 kV, 150 mA).

To clarify the fine structure characteristics of Fe_3Al intermetallic, further test was done by means of electron diffraction. TEM morphology and corresponding selected area electron diffraction pattern are shown in figure 5 (a, b). The electron diffraction pattern in figure 5b is a series of circles and has polycrystal diffraction characteristics.

According to the camera constant formula ($k = R_i d$), if we knew k and the diffraction circle radius, R_i, then the d value may be calculated by the formula

$$d_{cal} = k/R_i.$$

The results of the calculation and analysis are shown in table 4. The calculated value (d_{cal}) and standard value (d_{stan}) published by the Joint Committee on Powder Diffraction Standards (JCPDS) are identical. According to the characteristics of the polycrystal diffraction pattern, it can be determined that Fe_3Al intermetallic has very fine grain size.

The aluminized steel produced by the conventional HDA technology forms brittle layer (such as $FeAl_2$, $FeAl_3$, etc) on the surface, and it was easy to produce tiny cracks in the Fe–Al alloy layer and cannot bear larger stress and deformation. The conventional hot dip aluminizing process requires about 2 ~ 4 h, but this new hot dip aluminizing technology only requires about 10 ~ 15 min. The aluminized samples were treated by diffusion annealing (640°C × 30 min) and then cooled by slow cooling. A remarkable characteristic of this new aluminized steel is to eliminate brittle surface layer containing higher aluminum content. The deformation resistance of the aluminized steel may be greatly enhanced and the weldability was remarkably improved.

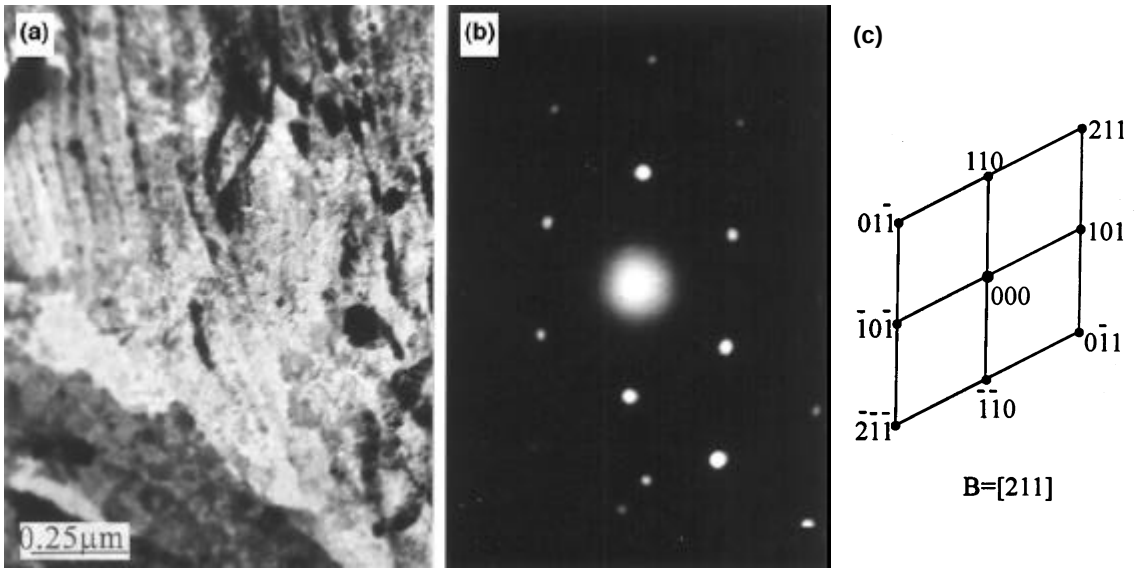

Figure 4. The fine structure characteristics of the Fe–Al alloy layer **(a)** TEM morphology, **(b)** electron diffraction pattern, and **(c)** schematic diagram.

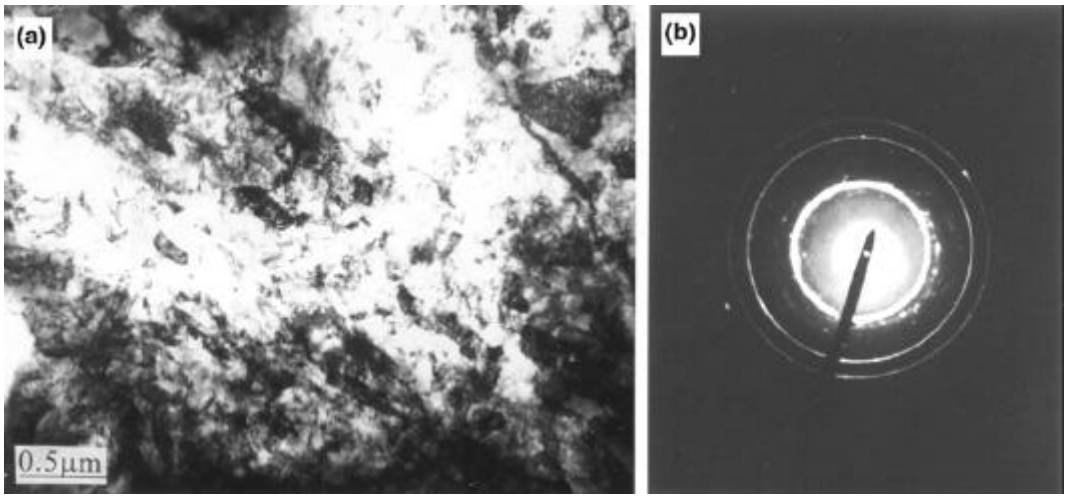

Figure 5. Microstructure of the Fe_3Al alloy layer **(a)** TEM morphology and **(b)** electron diffraction pattern.

Table 4. The calculated and analysed results of Fe_3Al electron diffraction pattern (k = 26·364).

Order of diffraction circles	R_i	d_{cal} (nm)	d_{stan} (nm)
1	7·91	0·333	0·334
2	9·06	0·290	0·289
3	12·76	0·206	0·204
4	14·65	0·180	0·179
5	–	–	0·167
6	118·2	0·145	0·145
7	22·3	0·118	0·118

The Fe–Al alloy layer obtained by this new HDA technology was Fe_3Al phase that had good toughness and lower hardness relatively. The aluminized steel obtained by this technology had certain ductility and ability to resist deformation. This is favourable for the engineering application of the aluminized steel.

4. Conclusions

(I) The thickness of the Fe–Al alloy layer on the surface of the new hot dip aluminized steel was 0·10 ~ 0·26 mm. The content of aluminum on the surface of the Fe–Al alloy layer was 32·7 ~ 36·6 wt%. The microhardness of the surface layer was HV 130 ~ 250, the microhardness of the sub-surface layer was HV 490 ~ 820, and then the microhardness in the coating reduced gradually.
(II) The Fe–Al alloy layer was composed of a-Fe (Al) solid solution, Fe_3Al (13·87% Al), FeAl (32·57% Al), Fe_2Al_5 (54·71% Al) with different proportions. There was no brittle phase containing higher aluminum content such as $FeAl_3$ (59·18% Al) and Fe_2Al_7 (62·93% Al). The tiny cracks and embrittlement, formerly caused by these brittle phases in the conventional aluminum-coated steel, were effectively eliminated. This is favourable for the application of the aluminized steel.
(III) The Fe–Al alloy layer of this new aluminized steel had the diffraction characteristics of the polycrystal and was composed of inlaid sub-grains. No microscopic defects (such as tiny cracks, pores or loose layer) were found in the Fe–Al alloy layer. This is favourable to resist high temperature oxidation and corrosion of the aluminized steel.

Acknowledgements

The work was supported by the Foundation of the National Key Laboratory of Advanced Welding Production Technology, Harbin Institute of Technology, and the National Foundation of the Natural Science (No. 50071028), PR China.

References

Bahadur A and Mohanty O N 1990 *Mater. Trans. JIM* **31** 948
Bahadur A and Mohanty O N 1991 *Mater. Trans. JIM* **32** 1053
Li Yajiang and Wang Xianli 1992 *Join. Sci.* **1** 100
Li Yajiang, Zhang Yonglan and Liou Yuxian 1995 *J. Mater. Sci.* **30** 2635
Li Yajiang, Wang Juan and Wu Huiqiang 2001 *Mater. Res. Bull.* **36** 2389
Tjong S C 1986 *Werkst. Korros.* **37** 591